A New Estimation Algorithm for the GNSS-R Interference Pattern Technique: The Segmented Maximum Likelihood

Miguel Angel Ribot, Cyril Botteron, Pierre-André Farine
École Polytechnique Fédérale de Lausanne (EPFL),
Electronics and Signal Processing Laboratory (ESPLAB), Switzerland

BIOGRAPHIES

Miguel Angel Ribot received his B.Sc. degree in telematics engineering from the Universitat de les Illes Balears (UIB), and his M.Sc. in information and communication technologies from Universitat Politècnica de Catalunya (UPC), in 2008 and 2011, respectively. He is currently working toward his Ph.D. in the Electronics and Signal Processing Laboratory (ESPLAB) at the École Polytechnique Fédérale de Lausane (EPFL), Switzerland. His Ph.D. is supported by the Swiss National Science Foundation (SNSF). His research interests include GNSS signal processing, and remote sensing using GNSS signals.

Dr. Cyril Botteron is leading, managing, and coaching the research and project activities of the Global Navigation Satellite System and Ultra-Wideband and mm-wave groups at École Polytechnique Fédérale de Lausanne (EPFL). He is the author or co-author of 5 patent families and over 90 publications in major journals and conferences in the fields of wireless positioning systems, GNSS-based navigation and sensing, ultra-low-power radio frequency communications and integrated circuits design, and base-band analog and digital signal processing.

Prof. Pierre-André Farine is professor in electronics and signal processing at EPFL, and is head of the electronics and signal processing laboratory. He received the M.Sc. and Ph.D. degrees in Micro technology from the University of Neuchâtel, Switzerland, in 1978 and 1984, respectively. He is active in the study and implementation of low-power solutions for applications covering wireless telecommunications, ultra-wideband, global navigation satellite systems, and video and audio processing. He is the author or co-author of more than 100 publications in conference and technical journals and 50 patent families (more than 270 patents).

ABSTRACT

During the last years, Global Navigation Satellite Systems (GNSS) reflectometry (GNSS-R) receivers have proven in several field experiments that GNSS signals reflected and scattered from the Earth's surface can be used in passive remote sensing applications. In ground based GNSS-R receivers, when the line-of-sight (LOS) signal coherently combines at then antenna with the reflected signal, the measured signal-to-noise ratio (SNR) will slowly fluctuate with the change of the GNSS satellite elevation. The Interference Pattern Technique (IPT) was proposed in order to use these SNR fluctuations to infer the distance between the antenna and the ground, as well as some of the geophysical properties of the nearby reflecting surface. The IPT implies little or no modification on the GNSS receiver, but it usually requires fairly long observation periods leading to a poor spatial resolution. Using the existing models, it is possible to express the reflected signal amplitude as a function of the height of the receiver antenna, the surface relative permittivity, and a surface roughness coefficient. Using the output of the receiver's prompt correlators, we propose a new computationally efficient optimization algorithm, the segmented maximum likelihood (SML), that makes use of the particular properties of the likelihood/cost function under consideration to obtain the maximum likelihood estimator (MLE). We also show, by computing the estimator's root-mean-square error and comparing it with the Cramér-Rao lower bound, how the obtained estimator can be efficient even for relatively short observation times.

I. INTRODUCTION

During the last decade, several experimental campaigns have demonstrated that Earth-reflected Global Navigation Satellite System (GNSS) signals observed at ground-based receivers can be used for passive remote sensing applications. This is usually referred as GNSS-reflectometry or GNSS-R (e.g. [1]–[4]). In such GNSS-R receivers, when the line-of-sight (LOS) signal coherently combines at the antenna with the reflected signal, the measured signal-to-

noise ratio (SNR) slowly fluctuates as a result of the constructive and destructive interference of the two signals that depend on the changing system geometry (since the satellite is moving on the sky), as well as on the geophysical properties of the nearby reflecting surface. The Interference Pattern Technique (IPT) makes use of these SNR variations for different applications such as ground altimetry, soil moisture and vegetation water content estimation, or even snow depth determination (e.g. [5]–[11]). One significant advantage of the IPT resides in the fact that it requires little to no modification of the GNSS receiver's signal processing architecture. As a consequence, applying the IPT on the large amount of SNR data available from the large number of already deployed geodetic receivers can enable the creation of a large network for soil moisture and snow/ice monitoring in a very cost-efficient way [12]. On the other hand, the IPT requires fairly long observation periods since the satellite's elevation has to change in order to induce a change in the SNR. Thus, depending on the antenna's height above the ground, the reflected signal's track will cover a relatively wide area over the reflection surface, which requires having a sufficiently homogeneous surface without any major obstacles over the signal's reflection track during a given observation period (typically a few minutes). In any case, GNSS-R can fill up an important gap between the spatial and temporal resolutions offered by current in-situ's instrumentations and space instrumentations [11].

In order to infer some characteristics of the reflecting surface using the IPT; an inversion model is required. In recent years, several signal models for the GNSS L-band multipath caused by different kinds of surfaces have been proposed. More specifically, in [13] the authors proposed a model for land reflections. This model describes the amplitude of the reflected signal as a function of a set of parameters: the height of the receiver antenna, the surface's relative permittivity (ε), and a surface roughness coefficient. ε is usually used as input for different empirical models to retrieve soil moisture [14], [15]. Using this model and the measured SNR data, or preferably, if it is available, the output of the receiver's correlators, it is possible to develop different estimators for these parameters.

Because of its simplicity and cost-effectiveness, the IPT technique has received some attention during the last years within the GNSS-R research community. However, there is still no consensus about the optimal estimation technique to retrieve the desired parameters from the observed noise interference pattern. E.g., in [16]–[18], each work considers the use of a different retrieval technique or set of techniques.

In this paper, we propose to use the maximum likelihood (ML) estimation technique. Unfortunately, for the signal model considered in Section II, which is analogous to the one proposed in [13], the ML estimator does not have a closed-form expression. In addition, this model is highly non-linear, thus computing directly the ML estimate leads to a computationally demanding optimization problem, especially for the joint parameter estimation. To overcome this limitation, in Section III, we propose a new computationally efficient optimization algorithm to compute the ML estimator, which relies on exploiting the particular properties of the likelihood/cost function under consideration. We have called this algorithm segmented ML (SML). In Section IV the performance of the proposed SML algorithm is assessed through simulations, by comparing its root-mean-square error (RMSE) with the Crámer-Rao lower bound (CRB).

II. SIGNAL MODEL FOR THE IPT

Here, we introduce a signal model for the measurements obtained from the receiver's prompt correlator complex output while tracking the GPS L1 C/A signal under the presence of a single coherent specular reflection. The height of the receiver antenna considered is small enough, such that the delay difference between the line-of-sight (LOS) component and the reflected component is lower than one code chip period, this is approximately 1 μs, or equivalently 300 m for GPS C/A code. Figure 1 shows the geometry of the considered scenario. We focus only on the case of a horizontal planar smooth and homogenous surface. As smooth surface, we assume that the standard deviation of its height (σ_{sh}), or surface roughness coefficient, satisfies the Rayleigh criterion [19], and that all the energy received was scattered from within the surface's first Fresnel zone, labeled as G_s in Figure 1. For simplicity, we assume that the satellite azimuth remains constant. Under this assumption, the satellite and the receiver will be contained within the same vertical plane over the entire measurement period.

The receiver tracking loop considered is the widely used combination of a delay lock loop (DLL) for the code tracking and a phase lock loop (PLL) for the carrier tracking [20]. We assume, without loss of generality, that the carrier frequency has been completely removed by the tracking loop since for a stationary receiver, both LOS and reflected components will experience the same Doppler shift [21]. Moreover, we also ignore the navigation data message in our analysis by assuming that the receiver has already achieved bit synchronization.

During the tracking stage, we can express the output of the prompt correlator at instant $t = nT$ as

$$x[n] = s_0[n] + s_1[n] + w[n], \qquad (1)$$

where $s_0[n]$ and $s_1[n]$ are the LOS and reflected components, respectively, and $w[n]$ is the zero-mean additive

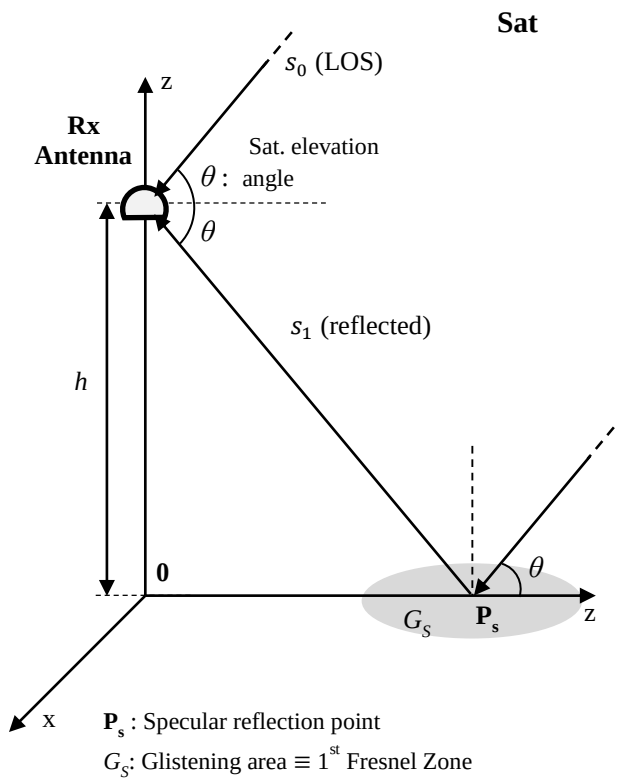

Figure 1 – Geometry of the scenario

white Gaussian noise (AWGN) term. Moreover, we can express the two signal components as

$$s_0[n] = u_0[n]F_R[n]\Lambda(\Delta\tau_0[n]), \tag{2}$$

$$s_1[n] = u_0[n]\Gamma[n]\Lambda(\Delta\tau_0[n] + \delta[n]c^{-1})\exp\{jk\delta[n]\}, \tag{3}$$

where:

- $u_0[n]$ is the complex amplitude of the LOS component that can be expressed as

$$u_0[n] \triangleq a_0 \exp\{j\Delta\phi_0[n]\} \tag{4}$$

  where a_0 is the LOS amplitude, which is assumed to remain constant over the entire observation period, which is not a strong assumption for short observation times, i.e. on the order of a few minutes, like the ones that we consider in this paper. $\Delta\phi_0[n]$ represents the difference between the true LOS carrier phase and one estimated by the tracking loop.
- $F_R[n]$ is the antenna complex amplitude gain for right-hand circular polarization (RHCP). It is a function of the received signal elevation and azimuth angles at any given instant.
- $\Lambda(\tau)$ is the C/A code autocorrelation function defined as [20], [22]

$$\Lambda(\tau) = \frac{1}{T}\int_{-T/2}^{T/2} c_f^*(t-\tau)c(t)\,dt, \tag{5}$$

  where $c(t)$ is the locally generated C/A code replica, and $c_f(t-\tau)$ is the received code delayed by τ, and filtered by the receiver's front-end. We assume that the front-end bandwidth is sufficiently large such that $c_f(t) \approx c(t)$.
- $\Delta\tau_0[n]$ is the code phase difference between the true LOS code phase and the one estimated by the tracking loop.
- $\delta[n]$ is the path difference between the LOS and the reflected component, in this case

$$\delta[n] = 2\,h\sin(\theta[n]) \tag{6}$$

  where h is the perpendicular distance between the reflection surface and the antenna phase center, which from now on will be referred just as receiver's height.
- $k = 2\pi/\lambda$ is the wavenumber, with λ being the GPS L1 signal wavelength (approx. 19.04 cm).
- $\Gamma[n]$ is the reflectivity coefficient, that will depend on the surface electrical properties and the signal incidence angle.

Depending on the surface considered, different models for $\Gamma[n]$ have been used to model the attenuation and phase shift observed on the reflected component for GPS L1 [8], [14], [23]. In this paper, we use the $\Gamma[n]$ model described in [13], proposed for a single layer bare-soil surface. We also use the same model for calm water surfaces. This model captures the depolarization of the GPS signal upon its reflection, the attenuation or loss of coherence due to the surface roughness, and the effect of the antenna radiation pattern. Thus, $\Gamma[n]$ can be expressed as

$$\Gamma[n] = g(\theta[n], \varepsilon, \sigma_{\mathrm{sh}}, F_{R/L}(\theta[n])). \tag{7}$$

It is thus a function of the satellite elevation ($\theta[n]$) changing over time, the surface relative permittivity, the surface roughness coefficient and the antenna pattern for RHCP and left-hand circular polarization (LHCP).

During the signal tracking, the presence of the coherent reflected component will introduce a bias in the estimated code phase delay and the carrier phase, i.e. $\Delta\tau_0[n] = b_\tau[n]$ and $\Delta\phi_0[n] = b_\phi[n]$. These biases will depend on the reflected component signal, as well as strongly on the receiver's tracking architecture considered. In this paper, for the sake of simplicity, we neglect these biases, i.e. $b_\tau[n], b_\phi[n] \approx 0$, under the assumption that they are small enough given a tracking architecture implementing some multipath mitigation scheme, such as narrow correlator or double delta correlator techniques [20], [24], [25].

Finally, given the slow rate of change of the satellite elevation, i.e. on the order of 10^{-3} degrees per second, we will reduce the number of samples by averaging the correlator outputs over a second. By doing so, we assume that the mean of $x[n]$ remains constant over each second. From now on, when referring to $x[n]$ we will be referring to the sample obtained after 1 second averaging.

III. THE SEGMENTED ML ALGORITHM

Given the signal model described by equations (1),(2) and (3) from the previous section, we propose to use a maximum likelihood estimator (MLE) to jointly estimate the vector of unknown parameters, $\boldsymbol{\xi}$, from the set of noisy measurements $\mathbf{x} = \left[x[0], x[1], \dots, x[N-1]\right]^T$. $\boldsymbol{\xi}$ can be defined as

$$\boldsymbol{\xi} \triangleq [a_0 \quad \boldsymbol{\beta}^T]^T, \tag{8}$$

where a_0 is the LOS component amplitude, and

$$\boldsymbol{\beta} \triangleq [\varepsilon_r \quad \varepsilon_i \quad h]^T \tag{9}$$

is a vector that groups the unknown parameters of the model that are not linear with the data measurements. ε_r, ε_i are the real and imaginary parts, respectively, of the surface permittivity, and h is the height of the receiver. The use of a MLE is motivated by its interesting properties. It is asymptotically unbiased and efficient given a sufficiently large data record or for high SNR [26]. In this paper, we consider fairly long data observation times, e.g. on the order of a few minutes, and high SNR, due to the 1 second averaging. Thus, the MLE appears to be well suited for this case.

The MLE of $\boldsymbol{\xi}$ is defined as

$$\hat{\boldsymbol{\xi}}_{\mathrm{ML}} = \arg\max_{\boldsymbol{\xi}} \{\ln p(\mathbf{x}; \boldsymbol{\xi})\}, \tag{10}$$

where the log-likelihood function, $\ln p(\mathbf{x}; \boldsymbol{\xi})$, is maximized. Our vector of data measurements can be modeled as $\mathbf{x} \sim \mathcal{CN}(a_0 \mathbf{s}(\boldsymbol{\xi}), \sigma_w^2 \mathbf{I})$, where $\mathbf{s}(\boldsymbol{\xi}) \triangleq a_0^{-1} E\{\mathbf{x}\}$ is the expected value of $\mathbf{x}$ normalized by a_0 and σ_w^2 is the noise variance. In this case, Eq. (10) becomes equivalent to

$$\hat{\boldsymbol{\xi}}_{\mathrm{ML}} = \arg\min_{\boldsymbol{\xi}} \{\|\mathbf{x} - a_0 \mathbf{s}(\boldsymbol{\xi})\|^2\} \tag{11}$$

since we are considering Gaussian noise. In this case the MLE becomes equivalent to the least squares estimator (LSE). Since a_0 is linear in the data, the MLE for a_0 has the following closed-form expression:

$$\hat{a}_{0\,\mathrm{ML}} = \left(\mathbf{s}(\boldsymbol{\beta})^H \mathbf{s}(\boldsymbol{\beta})\right)^{-1} \mathbf{s}(\boldsymbol{\beta})^H \mathbf{x}\Big|_{\boldsymbol{\beta}=\hat{\boldsymbol{\beta}}_{\mathrm{ML}}}. \tag{12}$$

Replacing this in Eq. (11) we obtain

$$\begin{aligned} \|\mathbf{x} - a_0 \mathbf{s}(\boldsymbol{\beta})\|^2\big|_{a_0=\hat{a}_{0\,\mathrm{ML}}} &= \mathbf{x}^H \mathbf{x} \\ &- \left(\mathbf{s}(\boldsymbol{\beta})^{\mathrm{H}} \mathbf{s}(\boldsymbol{\beta})\right)^{-1} \|\mathbf{x}^H \mathbf{s}(\boldsymbol{\beta})\|^2. \end{aligned} \tag{13}$$

By doing so, finding $\hat{\boldsymbol{\xi}}_{\mathrm{ML}}$ can be reduced to finding

$$\hat{\boldsymbol{\beta}}_{\mathrm{ML}} = \arg\min_{\boldsymbol{\beta}} f(\boldsymbol{\beta}), \tag{14}$$

where

$$f(\boldsymbol{\beta}) \triangleq -\left(\mathbf{s}(\boldsymbol{\beta})^{\mathrm{H}} \mathbf{s}(\boldsymbol{\beta})\right)^{-1} \|\mathbf{x}^H \mathbf{s}(\boldsymbol{\beta})\|^2. \tag{15}$$

Our cost-function, $f(\boldsymbol{\beta})$, is a non-linear, non-convex, multimodal scalar function of 3 variables. As a consequence, finding $\hat{\boldsymbol{\beta}}_{\mathrm{ML}}$ is clearly not straightforward. Simple grid search methods to obtain $\hat{\boldsymbol{\beta}}_{\mathrm{ML}}$ can be computationally very expensive, and the accuracy of the method will be linked to the step size of the grid. Since $f(\boldsymbol{\beta})$ presents many local minima, for an arbitrary initial value of $\boldsymbol{\beta}$, simple steepest descent algorithms are more likely to converge to a local minimum instead of the global minimum. Although a vast amount of optimization methods have been described in the literature (e.g. [27], [28]) to address these kind of optimization problems, in this paper we propose a simple alternative by taking advantage of the specific properties shown by $f(\boldsymbol{\beta})$.

In practice, we have spotted a strong quasi-periodic behavior of $f(\boldsymbol{\beta})$ in the h dimension. By fixing $\hat{\varepsilon}$ to its true value, i.e. $f(\boldsymbol{\beta})|_{\hat{\varepsilon}=\varepsilon} = f(h)$, we observed that the mean distance between local minima in h, d_h, can be approximated as

$$d_h \approx \frac{\lambda}{2}\left(\frac{1}{N}\sum_{n=0}^{N-1} \sin(\theta[n])\right)^{-1}. \tag{16}$$

To verify this periodicity, we computed the Discrete Fourier Transform (DFT) of $f(h)$ over 1000 Monte Carlo iterations for different ε values and satellite elevation spans. The results, depicted in Figure 2, show a peak approximately at d_h^{-1} for each of the considered cases. In agreement with Eq. (16), the position of the peak, and thus the periodicity of the local minima, does not seem to depend on the surface properties or the height of the receiver. For $f(\boldsymbol{\beta})$ this quasi-periodic behavior was also observed, together with a much smoother behavior of $f(\boldsymbol{\beta})$ in $\varepsilon_r, \varepsilon_i$ dimensions, i.e. for most of the $\boldsymbol{\beta}$ values, we have that

$$\frac{\partial f(\boldsymbol{\beta})}{\partial \varepsilon_{r/i}} \ll \frac{\partial f(\boldsymbol{\beta})}{\partial h}. \tag{17}$$

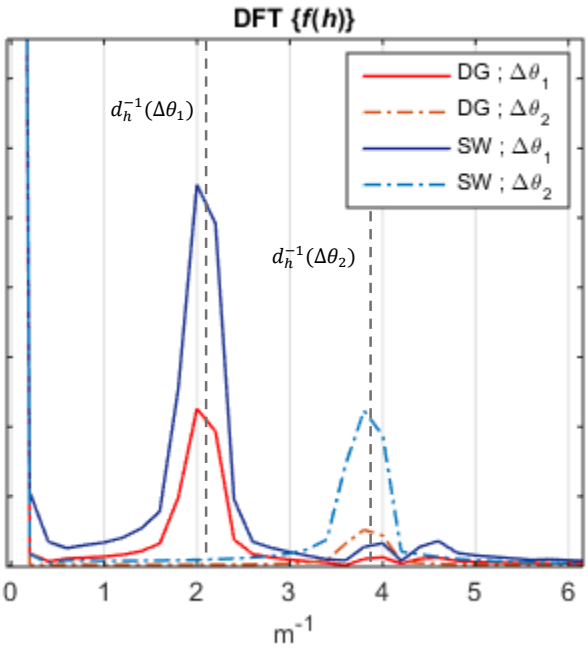

Figure 2 - Mean value of the magnitude of DFT of $f(h)$ for two different satellite elevation spans, $\Delta\theta_1$=[10º,13º] with $d_h(\Delta\theta_1) = 0.47$, and $\Delta\theta_2$=[20º, 23º], with $d_h(\Delta\theta_2) = 0.26$; for two different surface materials: dry ground (DG), with $\varepsilon_{DG} = 4 - j1.14$, and sea water (SW), with $\varepsilon_{SW} = 20 - j45.69$. In all four cases, $f(h)$ was generated for $\boldsymbol{x}$ with an LOS component SNR = 25 dB and 600 samples.

Since the distance between local minima can be roughly estimated in advance as d_h, we propose a new method or algorithm tailored to our particular $f(\boldsymbol{\beta})$ to compute $\widehat{\boldsymbol{\beta}}_{\mathrm{ML}}$, the segmented maximum likelihood (SML) algorithm. This algorithm is mainly based on two principles:

1. For any given scenario, it is reasonable to assume some knowledge of the range of values that $\boldsymbol{\beta}$ might take. Using this knowledge we can constrain our search space to $S \subset \mathbb{R}^3$, such that $\boldsymbol{\beta} \in S : \boldsymbol{\beta}_{\min} \leq \boldsymbol{\beta} \leq \boldsymbol{\beta}_{\mathrm{Max}}$.

2. We can divide or "segment" S into K subspaces, $\{S_k\}$, with their centers separated a d_h distance in the h dimension. Each S_k will contain a single local minimum of $f(\boldsymbol{\beta})$.

By applying these simple principles, we are able to divide or "segment" the original optimization problem into K simpler and faster to solve problems. Next, we proceed with the description of the proposed SML algorithm.

Algorithm description

Let us now describe the proposed SML algorithm. First, in an initialization stage we compute d_h for the satellite elevation span ($\Delta\theta$) covered during the data measurement period. In addition, we define S by fixing $\{\boldsymbol{\beta}_{\min}, \boldsymbol{\beta}_{\mathrm{Max}}\}$ according to the considered scenario. The number of subspaces, K, is obtained as

$$K = \left\lceil \frac{(h_{\max} - h_{\min})}{d_h} \right\rceil. \tag{18}$$

Then, an initial guess $\boldsymbol{\beta}_{\mathrm{init}} \in S$ is selected. S_0 is defined around $\boldsymbol{\beta}_{\mathrm{init}}$ such that

$$\boldsymbol{\beta} \in S_0 : \begin{cases} \varepsilon_{r_{\min}} \leq \varepsilon_r \leq \varepsilon_{r_{\max}}, \\ \varepsilon_{i_{\min}} \leq \varepsilon_i \leq \varepsilon_{i_{\max}}, \\ h_{\mathrm{init}} - \dfrac{d_h}{2} \leq h \leq h_{\mathrm{init}} + \dfrac{d_h}{2} \end{cases} \tag{19}$$

Now we compute the first local minimum $\widehat{\boldsymbol{\beta}}_0$, the nearest to $\boldsymbol{\beta}_{\mathrm{init}}$, as

$$\widehat{\boldsymbol{\beta}}_0 = \arg\min_{\boldsymbol{\beta} \in S_0} \{f(\boldsymbol{\beta})\} \tag{20}$$

using a gradient-descent like algorithm. After obtaining $\widehat{\boldsymbol{\beta}}_0$, we can define every S_k, with $k \in \{1,2,\ldots,K-1\}$, such that

$$\boldsymbol{\beta} \in S_k : \begin{cases} \varepsilon_{r_{\min}} \leq \varepsilon_r \leq \varepsilon_{r_{\mathrm{Max}}}, \\ \varepsilon_{i_{\min}} \leq \varepsilon_i \leq \varepsilon_{i_{\mathrm{Max}}}, \\ [h_k]_{\mathrm{lb}} \leq h \leq [h_k]_{\mathrm{ub}} \end{cases} \tag{21}$$

and

$$[h_k]_{\mathrm{ub/lb}} = h_{\widehat{\boldsymbol{\beta}}_0} + \left(m_k \pm \frac{1}{4}\right) d_h. \tag{22}$$

$m_k \in \mathbb{Z}$ is defined as the multiple of d_h separating $h_{\widehat{\boldsymbol{\beta}}_0}$ from the center of S_k in the h dimension. Then, $\widehat{\boldsymbol{\beta}}_k$ is computed just like $\widehat{\boldsymbol{\beta}}_0$, but with $\boldsymbol{\beta} \in S_k$ instead. Finally, the global minimum $\widehat{\boldsymbol{\beta}}_{\mathrm{ML}}$ is determined by selecting the $\widehat{\boldsymbol{\beta}}_k$ that minimizes $f(\boldsymbol{\beta})$. Figure 3 summarizes this algorithm description in a flowchart form.

In Figure 4, we show a graphical example of the segmentation performed by SML algorithm in the case of $f(h)$ for illustration purposes. The upper plot shows how many local minima $f(h)$ happen for an h range between 0 and 7 m, for a true receiver height of 2.25 m and a satellite elevation span $\Delta\theta$=[20º, 23º]. Notice the relatively small difference between the global minimum value of f and the near local minima. The bottom plot graphically shows the segmentation into different S_k computed by the SML on a zoomed section around the global minimum of the top plot.

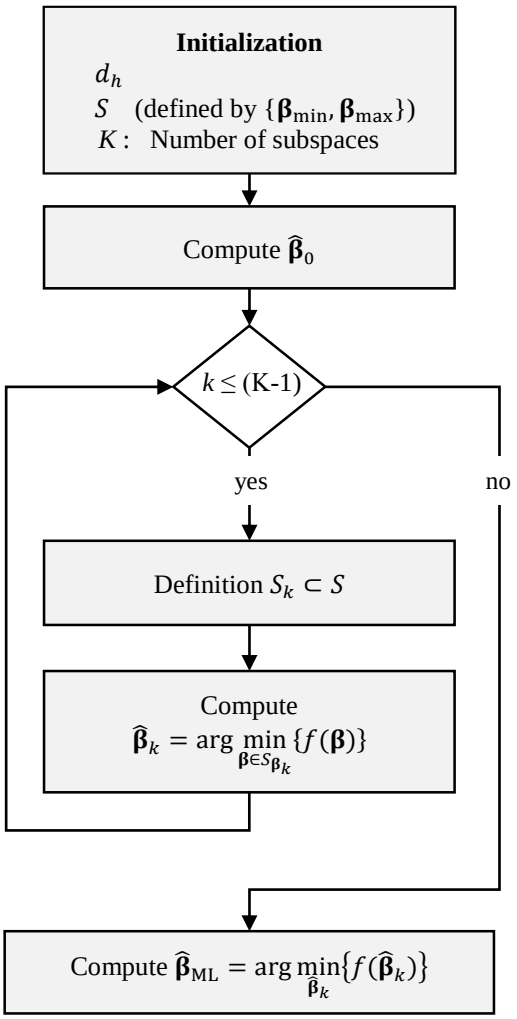

Figure 3 – SML algorithm flowchart

IV. PERFORMANCE ASSESSMENT

In this section we will assess the performance of the ML estimator computed using the proposed SML algorithm. To do so, we will estimate the root-mean-square error of the ML using Monte Carlo simulations for different cases. To validate the results obtained we will derive the Crámer-Rao lower bound for the IPT, considering the signal model previously introduced.

In all our simulations we considered a fixed antenna height of 2.25 m and an isotropic antenna, with an attenuation of 20 dB for the LHCP received signals. Two different surfaces have been considered, calm sea water, with an $\varepsilon_{\mathrm{SW}} = 20 - j45.69$, and dry soil, with $\varepsilon_{\mathrm{DG}} = 4 - j1.14 \cdot 10^{-4}$ [29]. In both cases σ_{sh} was fixed to $5 \cdot 10^{-3}$ m.

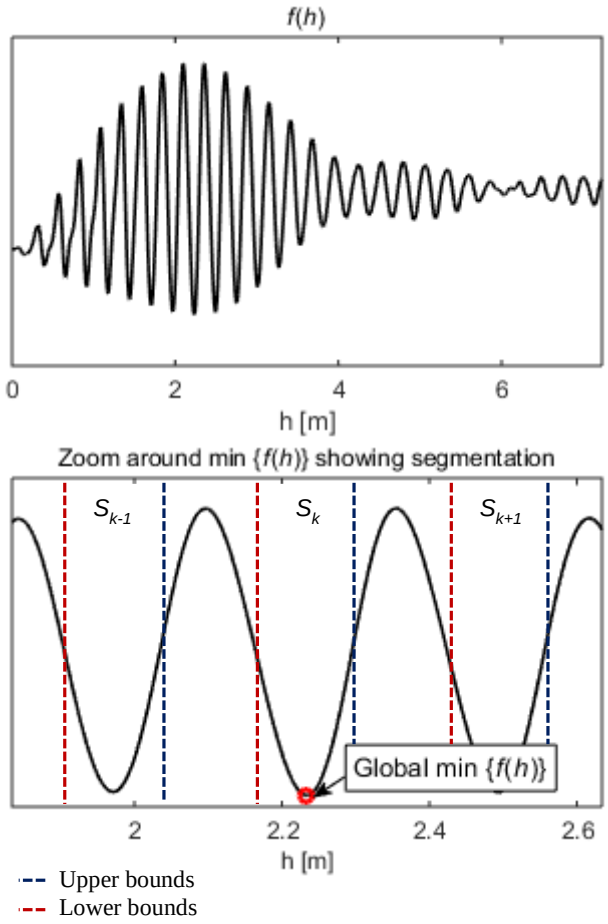

Figure 4 – (Top) Example of $f(h)$ evaluated for h = [0,7] m. $f(h)$ was generated for $\boldsymbol{x}$ with a LOS component SNR = 25 dB and 600 samples. (Bottom) Zoomed section around the global minimum of $f(h)$, showing the lower bounds (in red) and the upper bounds (in blue) computed by the SML to define every S_k subspace.

Crámer-Rao Lower Bound for IPT

A common approach to assess the performance of an unbiased estimator of a vector of unknown, but deterministic parameters, $\boldsymbol{\xi}$, is to compute the estimator's variance and compare it with the variance of the minimum variance unbiased (MVU) estimator, which is determined by the CRB [26]. As described before, the considered noisy data measurements, $\mathbf{x}$, can be expressed as

$$\mathbf{x} = \mathbf{s}(\boldsymbol{\xi}) + \mathbf{w}, \tag{23}$$

where

$$\mathbf{s}(\boldsymbol{\xi}) = E\{\mathbf{x}\}, \tag{24}$$

and $\mathbf{s}(\boldsymbol{\xi})$ represents the signal component, i.e. the s equations (2) and (3). Then, the Fisher Information Matrix (FIM) of $\boldsymbol{\xi}$, i.e. $\mathbf{J}(\boldsymbol{\xi})$ is defined as

$$[\mathbf{J}(\boldsymbol{\xi})]_{ij} = -E\left\{\frac{\partial^2 \ln p(\mathbf{x};\boldsymbol{\xi})}{\partial\xi_i \partial\xi_j}\right\}. \quad (25)$$

Since $\mathbf{w}$ is considered to be complex AWGN, according to [26], Eq. (25) reduces to

$$[\mathbf{J}(\boldsymbol{\xi})]_{ij} = \frac{2}{\sigma_w^2}\mathrm{Re}\left\{\frac{\partial \mathbf{s}^H(\boldsymbol{\xi})}{\partial\xi_i}\frac{\partial \mathbf{s}(\boldsymbol{\xi})}{\partial\xi_j}\right\}. \quad (26)$$

The CRB of each individual unknown parameter of $\boldsymbol{\xi}$, i.e. ξ_i when jointly estimating $\boldsymbol{\xi}$, is obtained as

$$\mathrm{CRB}(\xi_i) = [\mathbf{J}^{-1}(\boldsymbol{\xi})]_{ii} \quad (27)$$

In [5] a derivation for the CRB for the IPT was already described. However, a simpler signal model was used, where the reflectivity coefficient was assumed to be constant over the observation interval, only the magnitude of the correlator output was used as measurement, and only h and the amplitude a_0 were estimated.

SML performance evaluation with Synthetic Data

In order to validate the SML algorithm, and to verify the expected asymptotic behavior of the MLE, $\widehat{\boldsymbol{\beta}}_{\mathrm{ML}}$, obtained with it, we tested the algorithm for different satellite elevation spans lengths, $\Delta\theta$, ranging from 1.5º to 6º, but with all of them starting at the initial elevation θ_0 = 15º. For all $\Delta\theta$ a constant satellite elevation rate of $5\cdot10^{-3}$ º/s has been considered. We considered a single sample per second, obtained as described in section II. In this case, the number of samples will vary for each different $\Delta\theta$. For shortest span, $\Delta\theta$ = [15º, 16.5º], which corresponds to a total observation time of 5 min, we obtain 300 samples. For the rest of the spans, the number of samples will increase by multiples of 300 samples, until reaching 1200 samples for , $\Delta\theta$ = [15º, 21º], which corresponds to a total observation time of 20 min. Since the SNR of the received signal will vary due to the interference pattern observed, we defined instead

$$\mathrm{SNR}_0 \triangleq \frac{|a_0|^2}{\sigma_w^2}, \quad (28)$$

corresponding to the SNR that will be observed if only the LOS component was present. In our simulations, SNR_0 was set to a fixed value of 35 dB, which is a reasonable value considering the correlator output averaging performed over one second.

Figure 5, Figure 6, Figure 7 show the RMSE results obtained after Monte Carlo simulation, with M_{MC}1000 iterations for every elevation span for the estimates of ε_r, ε_i, and h, respectively. The signal model used to generate the noisy data was the one described in Section II. The RMSE estimate was computed for every span as

$$\mathrm{RMSE}(\widehat{\boldsymbol{\beta}}_{\mathrm{ML}}) = \sqrt{E\left\{\left|\widehat{\boldsymbol{\beta}}_{\mathrm{ML}} - \boldsymbol{\beta}\right|^2\right\}} \approx \sqrt{\frac{1}{M_{\mathrm{MC}}}\sum_{m=0}^{M-1}\left|\widehat{\boldsymbol{\beta}}_{\mathrm{ML}}[m] - \boldsymbol{\beta}\right|^2}. \quad (29)$$

As expected, the results show that the MLE computed with the SML algorithm is consistent, and shows the asymptotic behavior. In fact, it almost reaches the CRB for elevation spans of 3 º, i.e. 10 min observation time. Although the RMSE of the ε_r estimate almost attains the CRB even for the 1.5º elevation span, as shown in Figure 5 the error obtained will be too large for meaningful surface properties retrieval (e.g. soil moisture), at least with the assumed SNR_0 of 35 dB. In Figure 7, we observe how it is possible to reach sub-centimeter accuracy already with the $\Delta\theta$ = [15º, 18º]. The higher RMSE(h) value corresponding to the $\Delta\theta$ = [15º, 16.5º] can be explained due to the fact that not enough samples were considered to approximate the MLE asymptotic behavior.

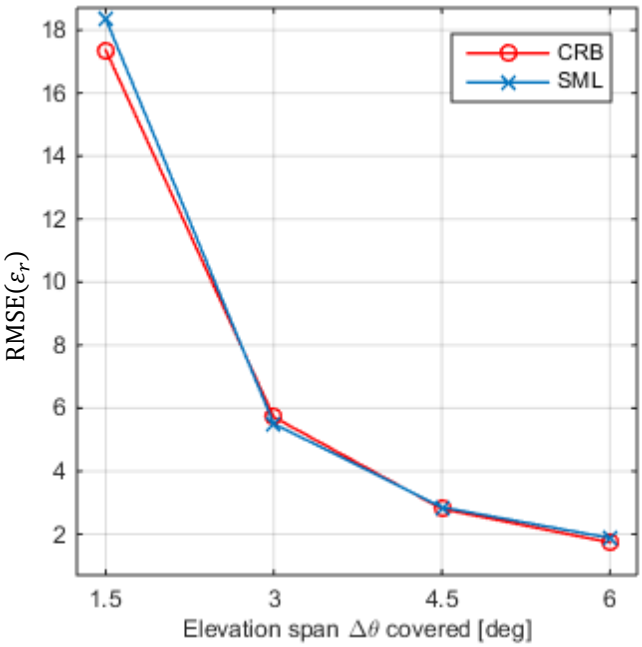

Figure 5 – RMSE of the ML estimate for the imaginary component of the surface permittivity, i.e. ε_r, computed using the SML compared with the $\sqrt{CRB}$ for the joint estimation of $\boldsymbol{\xi}$ for different elevation spans $\Delta\theta$ starting at an initial elevation θ_0 = 15º.

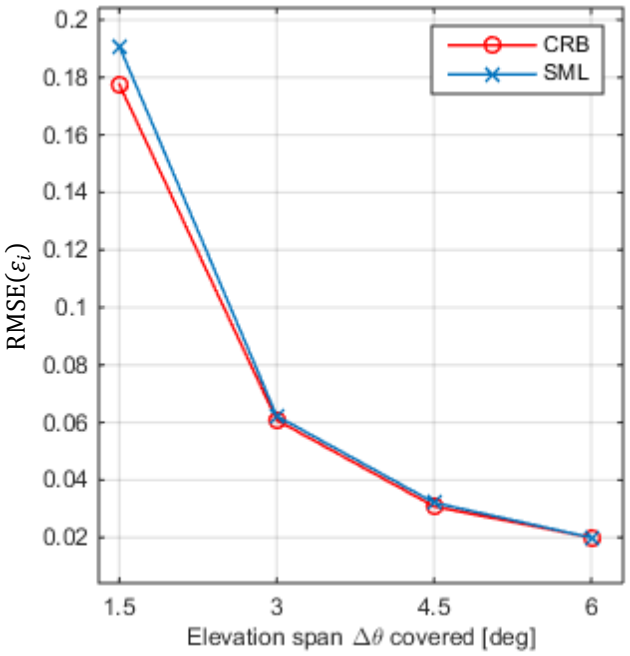

Figure 6 – RMSE of the ML estimate for the imaginary component of the surface permittivity, i.e. ε_i, computed using the SML compared with the $\sqrt{CRB}$ for the joint estimation of $\boldsymbol{\xi}$ for different elevation spans $\Delta\theta$ starting at an initial elevation θ_0 = 15º.

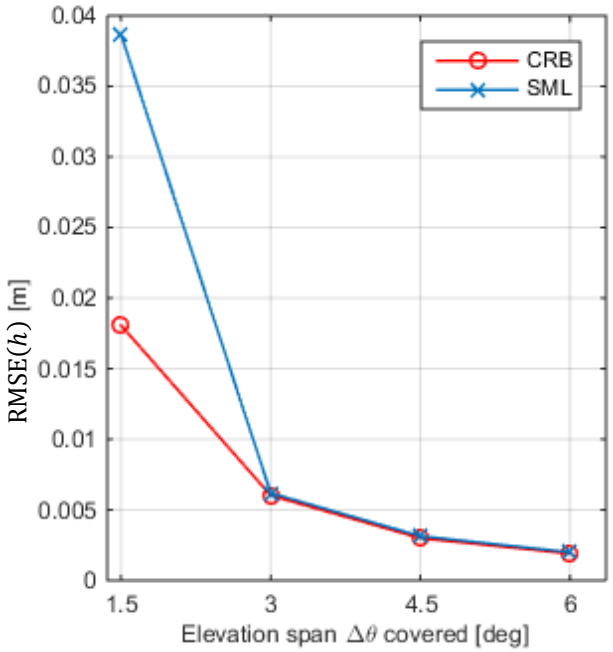

Figure 7 – RMSE of the ML estimate for the receiver's height, h, computed using the SML compared with the $\sqrt{CRB}$ for the joint estimation of $\boldsymbol{\xi}$ for different elevation spans $\Delta\theta$ starting at an initial elevation θ_0 = 15º.

V. CONCLUSION AND FUTURE WORK

This paper described the proposed SML algorithm, a computationally efficient way to obtain the MLE for the IPT signal model described in Section II. The SML algorithm, was validated using synthetic data generated using the same model with AWGN. As expected, the ML estimate obtained showed an asymptotically efficient behavior for satellite elevation spans equal or longer than 3º. This was verified by the matching of the estimated RMSE with the CRB, which was also computed for this signal model. By using the SML algorithm for long observation times, we seek to attain the optimal estimation accuracy for a given observation time, when considering an MVU estimator, or a significant reduction of the required observation time for a given estimation accuracy, which means a higher spatial and temporal resolutions. Although results seemed promising, the main weakness of the proposed MLE is that it strongly relies in the fitness of the model. Thus, the proposed estimator will be validated in future work using real measurements and by comparing its performance with other estimation methods used so far in practice. In addition, more simulations are planned after extending the signal model to include the effect of a realistic antenna pattern, to use other models for the reflectivity coefficient, and to model the receiver front-end bandwidth, as well as the bias not corrected by the tracking loop, present in the tracking estimates due to the presence of multipath.

ACKNOWLEDGMENTS

This work was supported by the Swiss National Science Foundation (SNSF) under grant no. 200020-153052.

REFERENCES

[1] K. M. Larson, E. E. Small, E. Gutmann, A. Bilich, P. Axelrad, and J. Braun, "Using GPS multipath to measure soil moisture fluctuations: initial results," *GPS Solut.*, vol. 12, no. 3, pp. 173–177, Aug. 2007.

[2] J. Dampf, T. Pany, N. Falk, B. Riedl, and J. Winkel, "Galileo Altimetry Using AltBOC and RTK Techniques," *Insid. GNSS*, vol. Jan/Feb, 2013.

[3] V. U. Zavorotny, S. Gleason, E. Cardellach, and A. Camps, "Tutorial on Remote Sensing Using GNSS Bistatic Radar of Opportunity," *IEEE Geosci. Remote Sens. Mag.*, vol. 2, no. 4, pp. 8–45, Dec. 2014.

[4] N. Rodriguez-Alvarez, A. Camps, M. Vall-llossera, X. Bosch-Lluis, A. Monerris, I. Ramos-

Perez, E. Valencia, J. F. Marchan-Hernandez, J. Martinez-Fernandez, G. Baroncini-Turricchia, C. Perez-Gutierrez, and N. Sanchez, "Land Geophysical Parameters Retrieval Using the Interference Pattern GNSS-R Technique," *IEEE Trans. Geosci. Remote Sens.*, vol. 49, no. 1, pp. 71–84, Jan. 2011.

[5] M. A. Ribot, J.-C. Kucwaj, C. Botteron, S. Reboul, G. Stienne, J. Leclère, J.-B. Choquel, P.-A. Farine, and M. Benjelloun, "Normalized GNSS interference pattern technique for altimetry.," *Sensors (Basel).*, vol. 14, no. 6, pp. 10234–57, Jan. 2014.

[6] R. N. Treuhaft, S. T. Lowe, C. Zuffada, and Y. Chao, "2-cm GPS altimetry over Crater Lake," *Geophys. Res. Lett.*, vol. 28, no. 23, pp. 4343–4346, Dec. 2001.

[7] A. Alonso Arroyo, A. Camps, A. Aguasca, G. F. Forte, A. Monerris, C. Rudiger, J. P. Walker, H. Park, D. Pascual, and R. Onrubia, "Dual-Polarization GNSS-R Interference Pattern Technique for Soil Moisture Mapping," *IEEE J. Sel. Top. Appl. Earth Obs. Remote Sens.*, vol. 7, no. 5, pp. 1533–1544, May 2014.

[8] K. M. Larson, J. J. Braun, E. E. Small, V. U. Zavorotny, E. D. Gutmann, and A. L. Bilich, "GPS Multipath and Its Relation to Near-Surface Soil Moisture Content," *IEEE J. Sel. Top. Appl. Earth Obs. Remote Sens.*, vol. 3, no. 1, pp. 91–99, Mar. 2010.

[9] M. Ozeki and K. Heki, "GPS snow depth meter with geometry-free linear combinations of carrier phases," *J. Geod.*, vol. 86, no. 3, pp. 209–219, Sep. 2011.

[10] K. M. Larson, E. D. Gutmann, V. U. Zavorotny, J. J. Braun, M. W. Williams, and F. G. Nievinski, "Can we measure snow depth with GPS receivers?," *Geophys. Res. Lett.*, vol. 36, no. 17, p. L17502, Sep. 2009.

[11] C. Botteron, N. Dawes, J. Leclère, J. Skaloud, S. Weijs, and P.-A. Farine, "Soil Moisture & Snow Properties Determination with GNSS in Alpine Environments: Challenges, Status, and Perspectives," *Remote Sens.*, vol. 5, no. 7, pp. 3516–3543, Jul. 2013.

[12] K. M. Larson, E. E. Small, E. D. Gutmann, A. L. Bilich, J. J. Braun, and V. U. Zavorotny, "Use of GPS receivers as a soil moisture network for water cycle studies," *Geophys. Res. Lett.*, vol. 35, no. 24, p. L24405, Dec. 2008.

[13] V. U. Zavorotny, K. M. Larson, J. J. Braun, E. E. Small, E. D. Gutmann, and A. L. Bilich, "A Physical Model for GPS Multipath Caused by Land Reflections: Toward Bare Soil Moisture Retrievals," *IEEE J. Sel. Top. Appl. Earth Obs. Remote Sens.*, vol. 3, no. 1, pp. 100–110, Mar. 2010.

[14] N. Rodriguez-Alvarez, X. Bosch-Lluis, A. Camps, M. Vall-llossera, E. Valencia, J. F. Marchan-Hernandez, and I. Ramos-Perez, "Soil Moisture Retrieval Using GNSS-R Techniques: Experimental Results Over a Bare Soil Field," *IEEE Trans. Geosci. Remote Sens.*, vol. 47, no. 11, pp. 3616–3624, Nov. 2009.

[15] M. S. Grant, S. T. Acton, and S. J. Katzberg, "Terrain Moisture Classification Using GPS Surface-Reflected Signals," *IEEE Geosci. Remote Sens. Lett.*, vol. 4, no. 1, pp. 41–45, Jan. 2007.

[16] F. G. Nievinski and K. M. Larson, "Inverse Modeling of GPS Multipath for Snow Depth Estimation—Part I: Formulation and Simulations," *IEEE Trans. Geosci. Remote Sens.*, vol. 52, no. 10, pp. 6555–6563, Oct. 2014.

[17] F. G. Nievinski and K. M. Larson, "Inverse Modeling of GPS Multipath for Snow Depth Estimation—Part II: Application and Validation," *IEEE Trans. Geosci. Remote Sens.*, vol. 52, no. 10, pp. 6564–6573, Oct. 2014.

[18] A. Alonso-Arroyo, A. Camps, H. Park, D. Pascual, R. Onrubia, and F. Martin, "Retrieval of Significant Wave Height and Mean Sea Surface Level Using the GNSS-R Interference Pattern Technique: Results From a Three-Month Field Campaign," *IEEE Trans. Geosci. Remote Sens.*, vol. 53, no. 6, pp. 3198–3209, Jun. 2015.

[19] W. G. Rees, *Physical Principles of Remote Sensing*. Cambridge University Press, 2012.

[20] E. D. Kaplan and C. J. Hegarty, *Understanding GPS: Principles and Applications*, 2nd ed. Artech House, 2006.

[21] S. Jin, E. Cardellach, and F. Xie, *GNSS Remote Sensing*, vol. 19. Dordrecht: Springer Netherlands, 2014.

[22] T. Pany, *Navigation Signal Processing for GNSS Software Receivers*. Artech House, 2010.

[23] A. Alonso-Arroyo, A. Camps, A. Aguasca, G. Forte, A. Monerris, C. Rudiger, J. P. Walker, H. Park, D. Pascual, and R. Onrubia, "Improving the Accuracy of Soil Moisture Retrievals Using the Phase Difference of the Dual-Polarization GNSS-R Interference Patterns," *IEEE Geosci. Remote Sens. Lett.*, vol. 11, no. 12, pp. 1–5, 2014.

[24] E. S. Lohan, R. Hamila, A. Lakhzouri, and M. Renfors, "Highly efficient techniques for mitigating the effects of multipath propagation in DS-CDMA delay estimation," *IEEE Trans. Wirel. Commun.*, vol. 4, no. 1, pp. 149–162, Jan. 2005.

[25] A. Jovanovic, Y. Tawk, C. Botteron, and P.-A. Farine, "Multipath mitigation techniques for CBOC, TMBOC and AltBOC signals using advanced correlators architectures," *IEEE/ION Position, Locat. Navig. Symp.*, pp. 1127–1136, May 2010.

[26] S. M. Kay, *Fundamentals of Statistical Signal Processing: Estimation Theory*. Englewood Cliffs, NJ: Prentice-Hall PTR, 1993.

[27] Z. Michalewicz and D. B. Fogel, *How to Solve It: Modern Heuristics*. Springer Berlin Heidelberg, 2013.

[28] A. Antoniou and W. S. Lu, *Practical Optimization: Algorithms and Engineering Applications*. Springer, 2007.

[29] B. Hannah, "Modelling and simulation of GPS multipath propagation," Queensland University of Technology, 2001.